Optics Communications 364 (2016) 60–66

Contents lists available at ScienceDirect

Optics Communications

journal homepage: www.elsevier.com/locate/optcom

Analysis of strain effects on the dynamic spectra of a quantum well semiconductor optical amplifier using quantum well transmission line modelling method

Mingjun Xia, H. Ghafouri-Shiraz *

School of Electronic, Electrical and System Engineering, University of Birmingham, Birmingham B15 2TT, UK

ARTICLE INFO

Article history:
Received 22 May 2015
Received in revised form
6 November 2015
Accepted 11 November 2015
Available online 21 November 2015

Keywords:
Strain effects
Dynamic spectra
Quantum well transmission line modelling method
Quantum well amplifiers
Femtosecond pulse amplification

ABSTRACT

This paper studies the strain (i.e. compressive (CS) and tensile (TS)) effects on the dynamic spectra of an amplified femtosecond pulse in a quantum well semiconductor optical amplifier (QW-SOA) using quantum well transmission line modelling (QW-TLM) method. Based on the analysis of band structure, the gain spectrum as well as the spontaneous spectrum of quantum well (QW) in the CS, unstrained (US) and TS are investigated using QW-TLM and it was found that in the CS QW, the magnitude ratio of the gain spectrum and the spontaneous emission spectrum is the largest. Furthermore, QW-TLM is adopted to investigate the dynamic spectral evolution of femtosecond pulse amplification in QW-SOAs and it was found that as the femtosecond pulse approaches the amplifier output, the centre frequency of the amplified femtosecond pulse spectra decreases and its bandwidth decreases. The output spectra of the amplified femtosecond pulse in QW amplifiers under the CS, US and TS cases are compared and the simulation results show that in a CS QW-SOA the spectral shape exhibits the largest magnitude and the smallest fluctuation due to the largest gain and the largest ratio between the gain and noise.

1. Introduction

Quantum well semiconductor optical amplifiers have been studied for applications in the long haul optical communications and all optical signal processing technology due to the small size, direct current pumping and wide nonlinear effects [1–6]. Compared with bulk SOAs, the increased dimensional confinement of carriers in the active region of QW amplifiers can reduce the gain recovery time [7,8]. Since the coupling among the heavy hole band, light hole band and the spin–orbit spilt-off band in the presence of strain becomes strong, the strain has a significant influence on the band structure and the refractive index of QW amplifiers. Existing theoretical and experimental work shows that both compressively stained (CS) and tensile strained (TS) QW amplifiers have superior characteristics as compared with the unstrained (US) QW amplifiers [9–11]. Some previous work studied the dynamic temporal and spectral characteristics of QW structures using the analytical expression method. The strain effects on the dynamic gain spectra in quantum well lasers were studied using the carrier and photon rate equations [12–14] and it was found that the bi-axial strain can effectively improve the gain characteristics and reduce the threshold current of quantum well lasers. The optical signal amplification in strained QW amplifiers suffers from the gain saturation effects [15–19], which leads to the temporal and spectral distortion due to the dynamic variations of the gain and spontaneous emission spectrum. In addition, many body effects induced by the carrier Coulomb interaction influences the gain and spontaneous emission spectra of strained quantum wells [20,21].

The quantum well transmission line modelling (QW-TLM) method [22] is an effective technique for analysis of semiconductor optical devices. It is based on the actual physical process of photon–electron interaction within the cavity which can be used to accurately study the properties of semiconductor optical devices both in the time and frequency domain. In the QW-TLM method, the electron transitions from the conduction band to the valence band in the wave vector space are represented by the parallel QW-TLM units. In each QW-TLM unit, two parallel RLC stub filters and the corresponding weight coefficients are adopted to model the electron transitions from the conduction band to the heavy hole band and the light hole band at a given vector. The method can provide the accurate description of optical processes by modelling the electron transition in semiconductor optical devices.

In this paper, the QW-TLM method is used to establish a model

* Corresponding author.
E-mail addresses: MXX322@bham.ac.uk (M. Xia), ghafourh@bham.ac.uk (H. Ghafouri-Shiraz).

http://dx.doi.org/10.1016/j.optcom.2015.11.033
0030-4018/

for strained QW amplifiers. The model consists of transmission line, transmission coefficient, spontaneous emission source and scattering module. The spontaneous emission and stimulated emission processes in QW amplifiers are represented by the spontaneous emission source and the scattering module. The band structures of QW amplifiers in the CS, US and TS cases have been analysed by considering the strain-dependent coupling between the heavy hole band, light hole band and spin–spilt off band. The different distributions of valence sub-bands are compared. The gain spectrum of the scattering module and the spontaneous emission spectrum of the spontaneous emission source in the model are obtained and compared in both strained and US cases. The evolution of the dynamic spectral shape of an amplified femto-second pulse along the amplifier cavity in the presence of compressive strain has been further investigated. Also, effects of strain on the output spectra of the amplified femto-second pulse have been studied based on QW-TLM.

The following paper is organized as: The theoretical model is introduced in Section 2. The strain effect on the band structure, gain and spontaneous emission spectrum of quantum well using QW-TLM is presented in Section 3. Comparisons of the dynamic spectra of the amplified pulse in the presence of CS, US and TS QW amplifiers are explained in Section 4 and conclusion is given in Section 5.

2. Theory

Fig. 1 shows the structure of the QW amplifiers model based on QW-TLM. The amplifier model is divided into m sections, each of which consists of scattering module, spontaneous emission source, transmission line and transmission coefficient α.

The input signal electric field $E_1(z, t)$ and that of the amplified spontaneous emission $E_2(z, t)$ propagate along the transmission line and arrive at the scattering module where the electric field stimulates the electron transitions. The spontaneous emission source and the scattering module describe the photon spontaneous and stimulated emissions processes. The internal structure of the scattering module is shown in Fig. 2.

In the scattering module, the input electric field $E_{in}(z, t)$ is converted into the input voltage signal V_{in} by the equation

$$V_{in} = E_{in}(z, t)\Delta L \tag{1}$$

where, ΔL is the length of the transmission line between two adjacent scattering modules. The input voltage propagates into the parallel QW-TLM units and scatters in the node of each stub filter. The amplified electric field $E_d(z, t)$ is obtained by the sum of the outputs of the parallel QW-TLM units multiplied by the gain coefficient G_0. The gain coefficient G_0 can be expressed as [23]:

$$G_0 = \frac{\Gamma q^2}{\pi h n_r c \varepsilon_0 m_0^2 L_z \gamma} \tag{2}$$

Where, Γ is the optical confinement factor, q is the magnitude of the electron charge, h is the Plank constant, c is the speed of light in free space, n_r and ε_0 are the refractive index and the permittivity in free space, m_0 is the electron rest mass in free space, L_z is the quantum well width, γ is the linewidth of the QW-SOA. The output electric field of the scattering module is given as

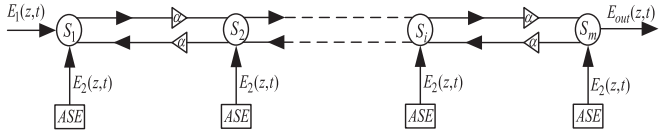

Fig. 1. The QW-TLM model.

$$E_{out}(z, t) = E_{in}(z, t) + E_d(z, t) \tag{3}$$

Each QW-TLM unit consists of two parallel RLC stub filters and the corresponding weight coefficients. In the ith QW-TLM unit, the first branch consists of the resistor Z_{ai}, the capacitor Z_{Cai} and the inductor Z_{Lai}, which are used to model the electron transition from the conduction band to the heavy hole band at a given wave vector while in the second branch the resistor Z_{bi}, capacitor Z_{Cbi} and inductor Z_{Lbi} are used to represent the electron transition from the conduction band to the light hole band at the wave vector $k_t(i)$. In the QW-TLM unit, the capacitors and inductors in the RLC filter have been modelled using the open-circuit and short-circuit transmission line [24]. The admittance expressions for the resistors (Y_{ai},Y_{bi}), capacitors (Y_{Cai},Y_{Cbi}) and inductors (Y_{Lai},Y_{Lbi}) can be expressed as [25]:

$$Y_{ai} = Y_{bi} = 1 \tag{4}$$

$$Y_{Cai} = \frac{1}{Z_{Cai}} = \frac{Q}{\tan(\pi f_1(k_t(i))\Delta T)} \tag{5}$$

$$Y_{Lai} = \frac{1}{Z_{Lai}} = Q\ \tan(\pi f_1(k_t(i))\Delta T) \tag{6}$$

$$Y_{Cbi} = \frac{1}{Z_{Cbi}} = \frac{Q}{\tan(\pi f_2(k_t(i))\Delta T)} \tag{7}$$

$$Y_{Lbi} = \frac{1}{Z_{Lbi}} = Q\ \tan(\pi f_2(k_t(i))\Delta T) \tag{8}$$

where

$$f_1(k_t(i)) = (E_n^c(k_t(i)) - E_{\sigma,m}^h(k_t(i)))/h \tag{9}$$

$$f_2(k_t(i)) = (E_n^c(k_t(i)) - E_{\sigma,m}^l(k_t(i)))/h \tag{10}$$

Q is the Q-factor of the stub filter, ΔT is the propagation time between two adjacent scattering modules ($\Delta T = 1/f_{sam}$ where f_{sam} is the sampling frequency), $E_n^c(k_t)$, $E_{\sigma,m}^h(k_t)$ and $E_{\sigma,m}^l(k_t)$ are the conduction band, the heavy hole band and the light hole band, respectively, which are obtained by solving the following Schrodinger equations [26,27]:

$$H^c\varphi_n(z; k_t) = E_n^c(k_t)\varphi_n(z; k_t) \tag{11}$$

$$\sum_{\upsilon=HH,LH} H_{3\times3,i\upsilon}^{\sigma} g_{m,\upsilon}^{\sigma}(z; k_t) = E_{\sigma,m}^{\upsilon}(k_t) g_{m,i}^{\sigma}(z; k_t) \tag{12}$$

where, H^c and $H_{3\times3,i\upsilon}^{\sigma}$ are the Hamiltonians for the conduction and valence bands, $\varphi_n(z; k_t)$ and $g_{m,\upsilon}^{\sigma}$ are the envelope functions of the nth conduction sub-band and the mth valence sub-band. In each QW-TLM unit, the weight coefficients A_i and B_i are given as [22]:

$$A_i = \frac{1}{f_1(k_t(i))} \left|\hat{e} M_{nm}^{\sigma\eta}(k_t(i))\right|^2 \times (F_n^c(k_t(i)) - F_{\sigma m}^h(k_t(i)))k_t(i)dk_t \tag{13}$$

$$B_i = \frac{1}{f_2(k_t(i))} \left|\hat{e} M_{nm}^{\sigma\eta}(k_t(i))\right|^2 \times (F_n^c(k_t(i)) - F_{\sigma m}^l(k_t(i)))k_t(i)dk_t \tag{14}$$

where, $M_{nm}^{\eta\sigma}(k_t(i))$ is the momentum matrix element for the stimulated emission in the wave vector $k_t(i)$, $F_n^c(k_t(i))$, $F_{\sigma m}^h(k_t(i))$ and $F_{\sigma m}^l(k_t(i))$ are the values of the Fermi–Dirac distribution function

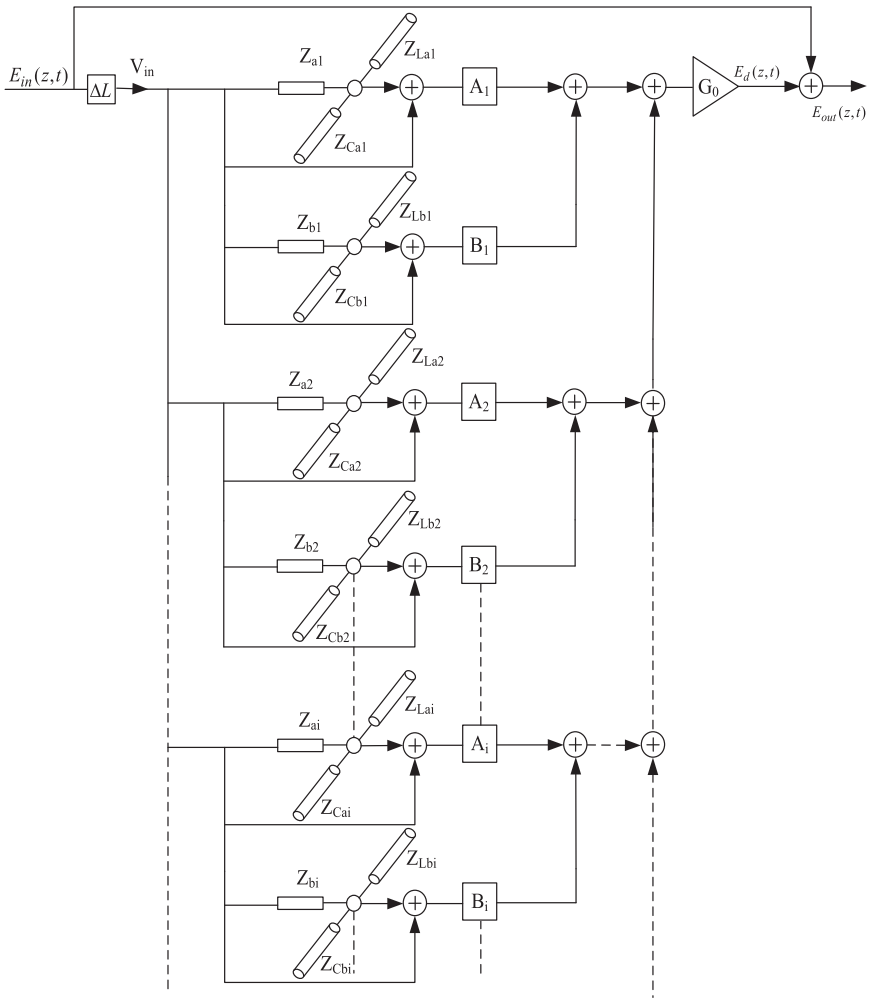

Fig. 2. Scattering module model.

for the conduction band, heavy hole band and light hole band at the wave vector $k_t(i)$, respectively [28]. The Q-factor in (Eqs. (5)–8) is given as:

$$Q = 2\pi f_m/\gamma \tag{15}$$

where, f_m is the central frequency of the QW-SOA. The increased carrier density will lead to the bandgap shrinkage due to many body effects [20,21], which means the central frequency of each Q-TLM unit decreases. The variations of the central frequency and the corresponding weight coefficient of each QW-TLM unit induced by the band structure renormalization due to many body effects have been neglected in this paper and will be included in the future work.

Fig. 3 shows the internal structure of the spontaneous emission source in the model which consists of an ASE source S_{ASE}, parallel QW-TLM units and the coupling coefficient β. The ASE source generates the spontaneous emission signal S_{ASE}, which can be expressed as [22]:

$$S_{ASE}(t) = \begin{cases} E_0\Delta L & \text{for} \quad t = nT_1,\ n = 0, 1, 2\ldots \\ 0 & \text{for} \quad (n-1)T_1 \le t \le nT_1,\ n = 1, 2\ldots \end{cases} \tag{16}$$

where, E_0 is the energy of a photon, T_1 is the lifetime in the exited state. In the spontaneous emission module, the admittance expressions in each QW-TLM unit are the same as those in the scattering module. The weight coefficients C_i and D_i in each QW-TLM unit can be expressed as [22]

$$C_i = S_0 f_1(k_t(i))\left|M_{sp}(k_t(i))\right|^2 \times f_n^c(k_t(i)) \times (1 - f_{\sigma m}^h(k_t(i)))k_t(i)dk_t \tag{17}$$

$$D_i = S_0 f_2(k_t(i))\left|M_{sp}(k_t(i))\right|^2 \times f_n^c(k_t(i)) \times (1 - f_{\sigma m}^l(k_t(i)))k_t(i)dk_t \tag{18}$$

where,

$$S_0 = \frac{8q^2 n_r^2 \Delta V}{h^2 c^4 \epsilon_0 m_0^2 L_z} \tag{19}$$

$M_{sp}(k_t(i))$ is the momentum matrix element of the spontaneous emission in the wave vector $k_t(i)$ [11], $\Delta V$is the volume of each section of the amplifier cavity.

The carrier density rate equation in each section of the amplifier cavity can be expressed as

$$\frac{dN}{dt} = \frac{I}{qV_{act}} - \frac{N}{\tau_s} - \frac{\Gamma}{qDW\Delta L}\frac{V_{in}}{Z_p} \tag{20}$$

where, I is the injected current, V_{act} is the volume of the active area, Z_p is the transverse wave impedance [29], V_{in} is the input voltage of each scattering module and is obtained by Eq. (4), the carrier-density dependent carrier recommendation lifetime τ_s is given by $[A + BN + CN^2]^{-1}$ where, A, B and C are linear recombination constant, Bi-molecular recombination constant and Auger recombination constant, respectively.

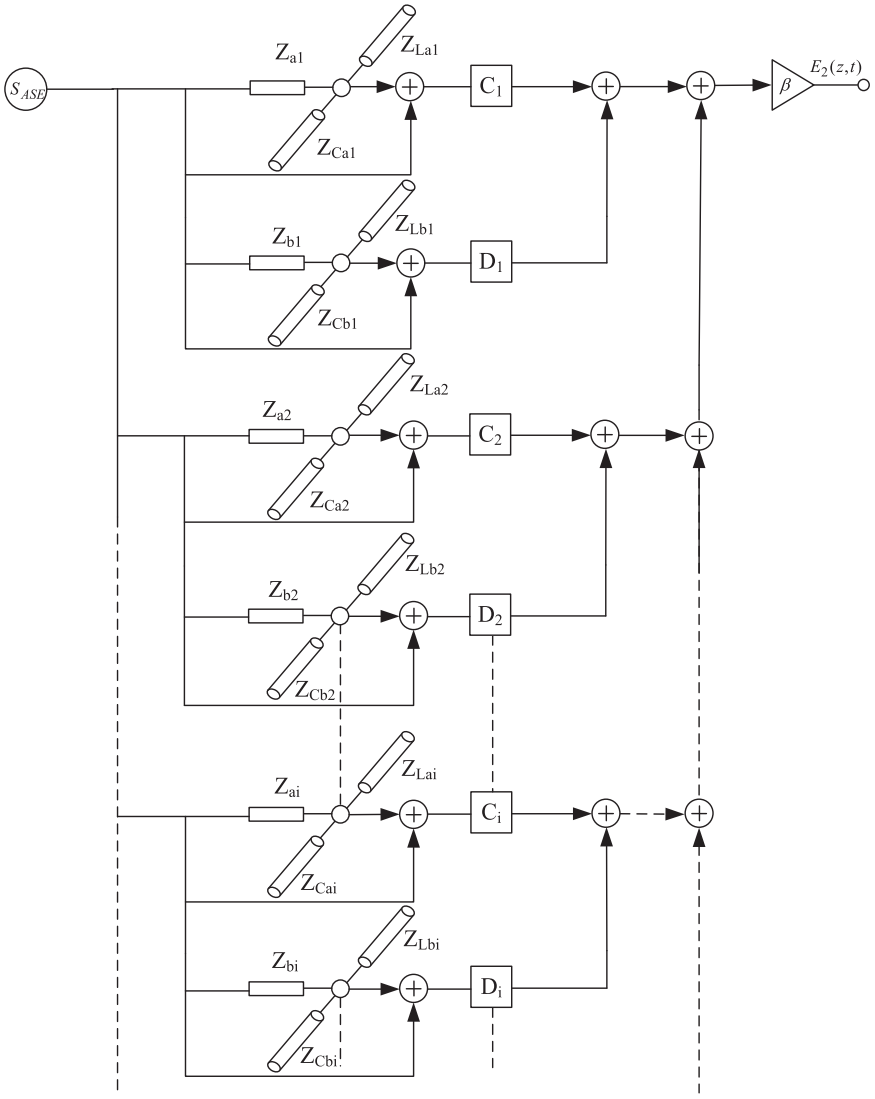

Fig. 3. Spontaneous emission source model.

3. Effects of strain on the QW-SOA properties

In the following, we have analysed the electronic and optical properties of the *InGaAs–InGaAsP* QW-SOA. The sub-band energy of the strained quantum well are calculated using the electron–photon interaction Hamiltonian considering the coupling among the heavy and light hole bands as well as the spin–orbit spilt-off band. Based on quantum well transmission line modelling (QW-TLM) method we have studied the gain and spontaneous emission spectra of strained quantum well amplifiers. Also, the dynamic spectra of an amplified femtosecond pulse have been investigated. Table 1 shows values of different parameters used in our simulations.

Table 1
Parameters used in the analysis.

Symbol	Description	Value
n	Background refractive index	3.67
f_{sam}	Sampling frequency	1.0×10^{15} Hz
A	Linear recombination	2×10^{8} s^{-1}
B	Bi-molecular recombination	6×10^{-16} m^{3}s^{-1}
C	Auger recombination	8×10^{-41} m^{6}s^{-1}
γ	Linewidth of QW-SOA	2×10^{13} rad/s
Γ	Confinement factor	0.025
N_0	Transparent carrier density	1.2×10^{24} m^{-3}
W	SOA width	1 μm
D	SOA thickness	24.5 nm

3.1. Band Structure of QW Amplifiers

Fig. 4 shows the valence band structures of $In_{1-x}Ga_xAs - InGaAsP$ QW amplifiers for the CS ($x = 0.3$), US ($x = 0.47$) and TS ($x = 0.65$) cases. The well is $In_{1-x}Ga_xAs$ with 4.5 nm width and the barrier is *InGaAsP* with a bandgap wavelength of 1.15μmas the barrier lattice matched to the *InP* substrate. From Fig. 4, it can be found that for the CS and US cases, the first heavy hole band lies above the first light hole band. However, the first light hole band lies above the first heavy hole band in the TS case. This is because in the CS and US cases the heavy hole has a larger effective mass along the growth direction. As the molar fraction of Gallium$x$increases, at the zone centre the heavy hole is moved to the lower energy while the light hole is moved to the higher energy due to the shear deformation potential. At the zone centre the CS QW-SOA has the largest energy spacing between the first two valence bands. It is clear that strain has induced different valence band structures in the QW amplifier, which causes the

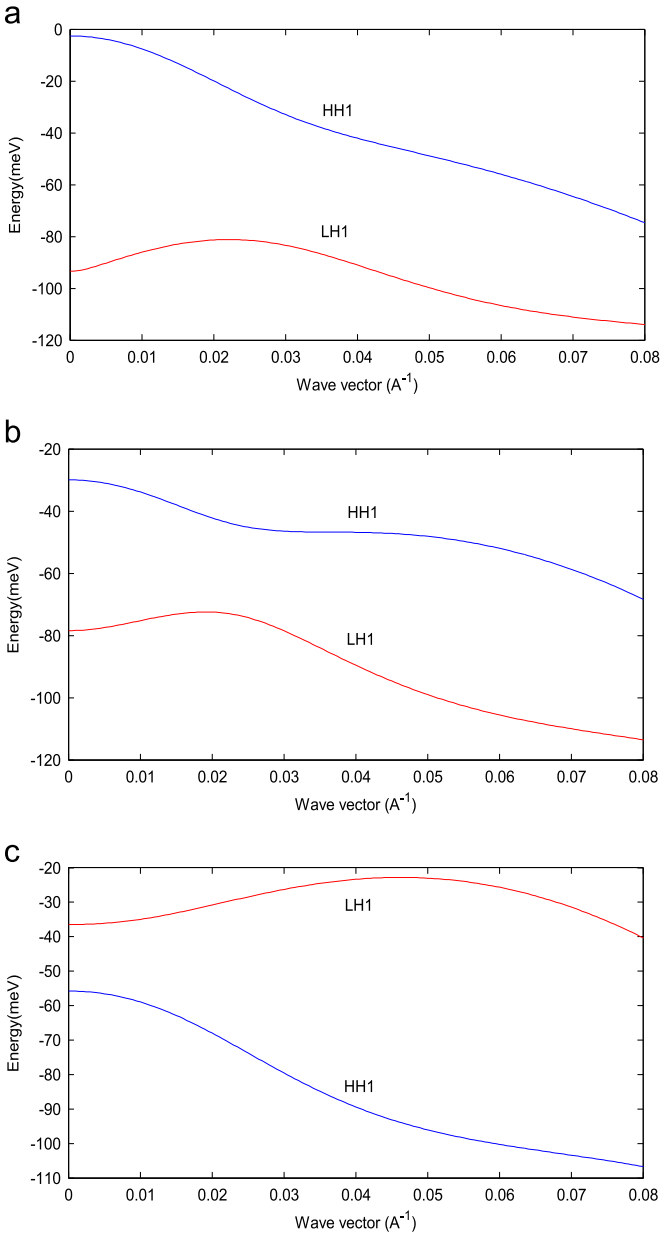

Fig. 4. Valence band structure of QW amplifiers (a) CS (b) US and (c) TS.

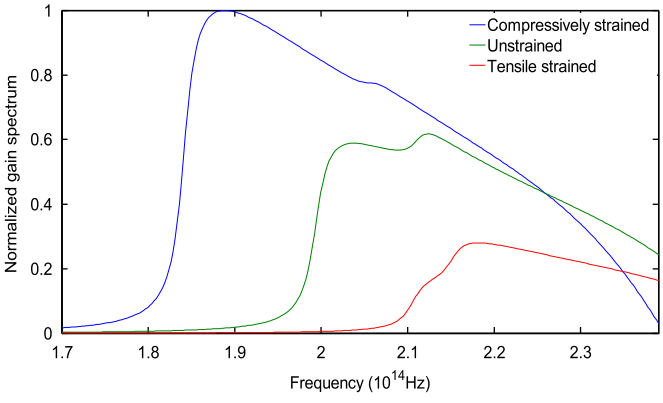

Fig. 5. Normalized gain spectra of QW amplifiers for three strained cases (CUT) at the carrier density 8×10^{24} m^{-3} obtained by the scattering module in the QW-TLM model.

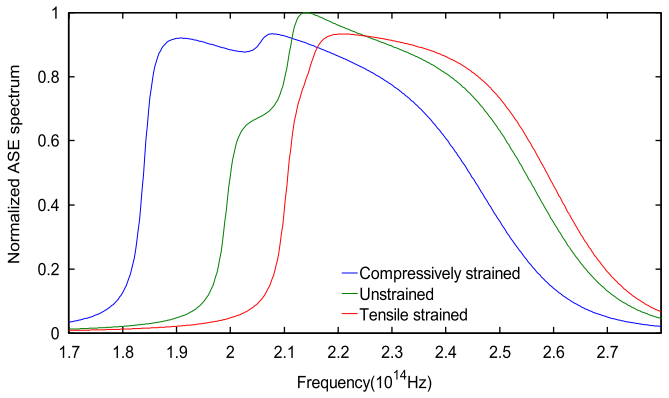

Fig. 6. Normalized spontaneous emission spectra of QW amplifiers for the three strained cases (CUT) at the carrier density 8×10^{24} m^{-3} obtained by the spontaneous emission source in the QW-TLM model.

centre frequency of the stub filter and the corresponding weight coefficients of each QW-TLM unit to change (see Fig. 3 and (Eqs. (9)–18)). Thus, the stimulated and spontaneous emission processes occurring in the scattering modules as well as the spontaneous emission source are different in three strained cases as shown in Figs. 5 and 6.

3.2. Gain and spontaneous emission spectra

Fig. 5 shows the normalized gain spectra of the strained QW amplifier. The FWHMs of the normalized gain spectra are 39.06, 36.13 and 30.52 THz, respectively, for CS, US and TS (CUT) while their central wavelengths are 188.72, 203.86 and 218.26 THz, respectively, which indicates a decrease in the gain bandwidth and a blue shift in gain central wavelength as the strain changes from compressive to tensile. This is because as the molar fraction of Gallium x increases, the first heavy hole is moved to the lower energy level while the first light hole is moved to the higher energy level. In the three strained cases, the magnitudes of the normalized gain spectra are 1, 0.6175 and 0.2799, respectively. Fig. 6 shows the normalized spontaneous emission spectra of the QW amplifier under different strained. The central frequencies of the spontaneous emission spectra for CUT cases are 207.76, 213.87 and 220.95 THz, respectively, while the FWHMs of the spontaneous emission spectra are 62.01, 54.93 and 49.56 THz. In contrast with the gain spectra, the magnitude of the spontaneous emission spectra in CUT are almost the same (0.9334, 1 and 0.9328). Further comparison of the gain and spontaneous emission spectra shows that the CS QW amplifier has the highest ratio between the gain and the spontaneous emission spectra magnitudes.

Fig. 7 shows the normalized gain spectra of a CS QW amplifier at different carrier densities. The results show that as the carrier density decreases from 7×10^{24} m^{-3} to 5×10^{24} m^{-3} the normalized gain reduces from 1 to 0.8 and also the bandwidth of the gain spectrum reduces from 34.18 to 22.95 THz and the centre frequency shifts from 188.23 to 187.74 THz.

4. Dynamic spectral analysis in the femtosecond pulse amplification

The envelope function of the input electric field in the time domain is a Gaussain pulse centred at 90 fs with the peak power and FWHM values of 1 mw and 60 fs, respectively. The corresponding central frequency and 3-dB bandwidth of the input signal in the frequency domain are 193.48 and 7.6 THz. This input signal is applied into a CS ($x = 0.3$) QW-SOA.

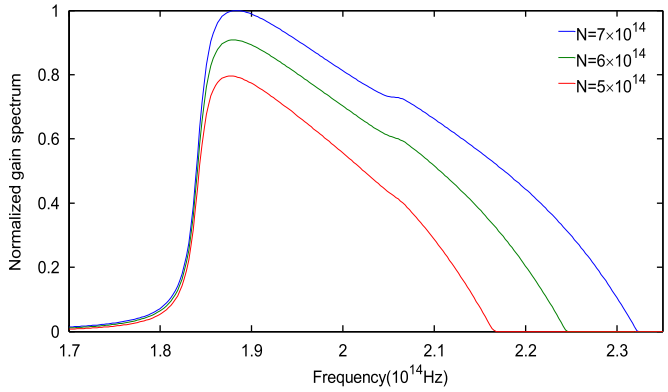

Fig. 7. Normalized gain spectra of the CS QW amplifier at three different carrier densities obtained by the scattering module in the QW-TLM model.

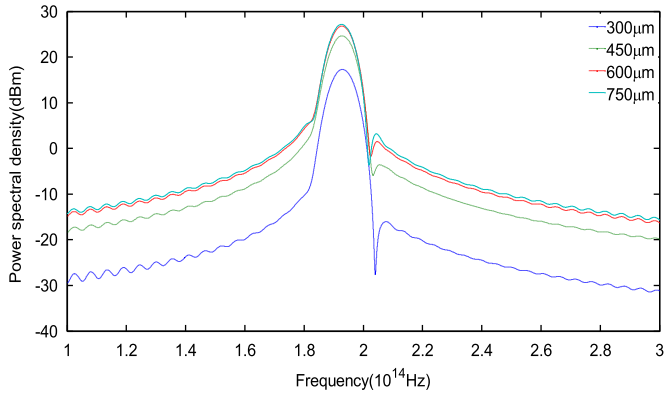

Fig. 8. Evolution of the amplified pulse spectral shapes along the amplifier cavity in the CS QW-SOA.

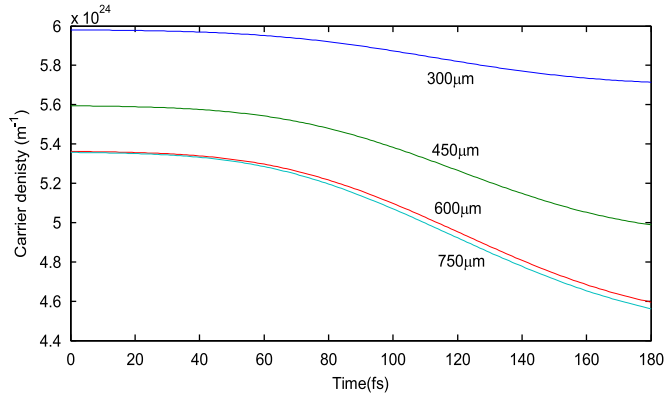

Fig. 9. Variations of carrier densities at different distances along the amplifier cavity during the pulse amplification in the CS QW amplifier.

Fig. 8 shows the evolution of the amplified pulse spectral shapes along the amplifier cavity. The results show that the peak value of the power spectra density increases (i.e. from 17.29 dBm at 300 μm to 27.04 dBm at 750 μm) as the pulse propagates towards the output facet of the amplifier while the central frequencies decreases from 193 to 192.72 THz (i.e. red shift). Also, the 3 dB bandwidth of the power spectral densities decreases from 7.404 to 7.001 THz. This is because as the distance increases, the input signal amplifies more which results in an increase in the magnitude of the power spectral density and the reduction of carrier density (see Fig. 9). Fig. 7 reveals that as the carrier density decreases, the gain spectra bandwidth reduces and the central frequency shifts to the smaller frequency.

Fig. 9 shows the variations of the carrier density during

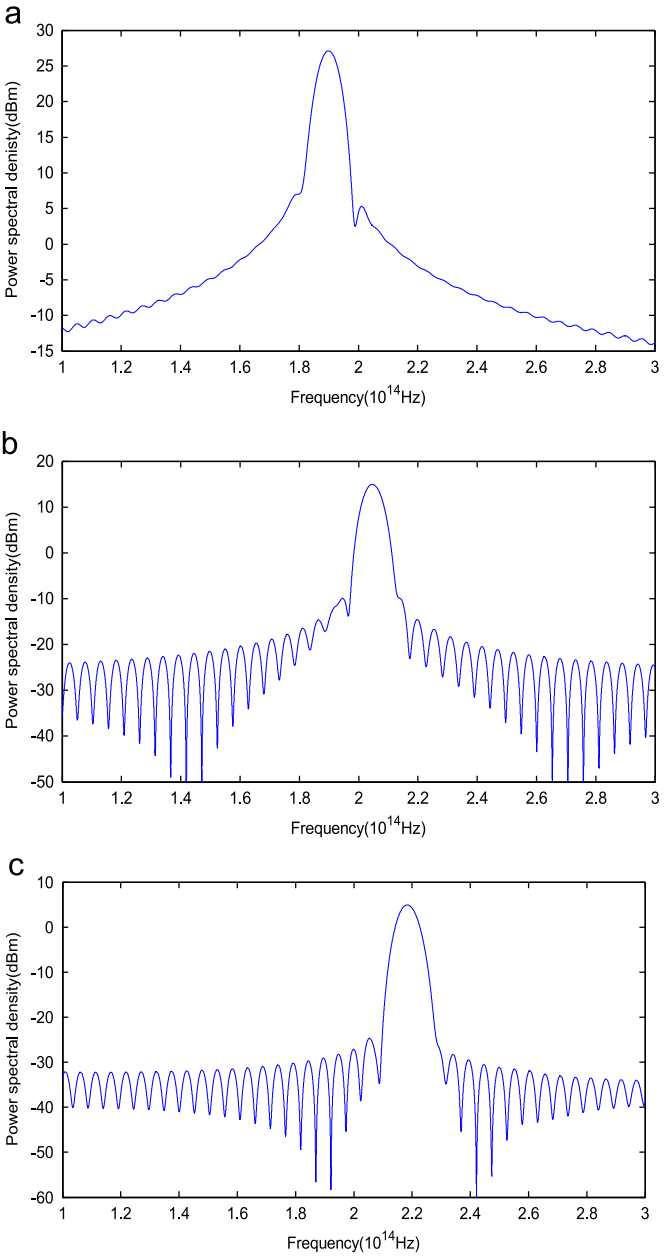

Fig. 10. Output spectra of the amplified femtosecond pulse (a) CS, (b) US and (c) TS.

femtosecond pulse amplification in a CS QW amplifier at different distances along the amplifier cavity. As the figure shows the carrier density decreases as the amplified pulse approaches the output facet of the amplifier. It should be noted that as the distance increases the noise intensity increases too. Thus, when the input pulse signal arrives at the corrponding distance, the initial carrier densies at $t = 0$ are different. Fig. 10 shows the effect of strain (compressive and tesile) on the output power spectral density of the amplified femtosecond pulse. In order to compare the effect of strain on dispersion of the amplified output pulse we have set the centre frequencies of the input signals at 188.72, 203.86 and 218.26 THz for CS, US and TS, respectively, which correrspond to the centre frequencies of their gain spectra. It was found in all cases the amplified output pulse has narrower bandwidth that as compared to the input pulse and red-shift in the centre frequency.

In the CS, US and TS QW amplifiers, the centre frequency shifts of the amplified output spectra with respect to the input spectra are 1.231, 0.790 and 0.113 THz, respectively. This is due to the fact

that in the CS QW amplifier the gain value around the centre frequency is the largest (see Fig. 5) which implies that the input signal is highly amplified during its propagation within the amplifier cavity and hence, the average carrier density level is lower, which induces a larger red shift. The magnitudes of the output power spectral density in the CS, US and TS cases are 27.11, 14.94 and 4.93 dBm, respectively. In the CS case, the variations of the 3 dB spectral bandwidths is 0.638 THz while in the US and TS cases, they are 0.529 and 0.424 THz, respectively. This is because in the CS case, the highest optical filed in the amplifier cavity leads to the lowest carrier density level, which suppresses the bandwidth of the gain spectrum. Also, the output spectral shape of the amplified femtosecond pulse in the CS QW amplifier shows the smallest fluctuation. This is because CS QW has the largest magnitude ratio between the gain spectrum and the spontaneous emission spectrum in the three (CS,US and TS) QWs cases (as shown Figs. 5 and 6).

5. Conclusion

In this paper, based on the quantum well transmission line modelling method we have analysed (i) the effect of strain on the band structure, gain and spontaneous spectra of QWs and (ii) the dynamic spectral behaviour of strained QW amplifiers. Simulation results show that in the CS QW amplifier offers a bigger ratio between the gain and the spontaneous emission spectra magnitudes as compared with US and TS QW amplifiers. As the carrier density decreases the magnitude and the bandwidth of the gain spectra reduces and the centre frequency shifts to a smaller frequency. Also, it was found that as the distance approaches to the amplifier length, both the centre frequency and the bandwidth of the amplified pulse spectra decrease and the CS QW amplifier exhibits the best output spectral properties (i.e.the highest magnitude and the lowest spectra fluctuations).

References

[1] J.M. Dailey, T.L. Koch, Simple rules for optimizing asymmetries in SOA-based Mach–Zehnder wavelength converters, IEEE J. Lightwave Technol. 27 (2009) 1480–1488.
[2] Zheng Xi Huang, Cui Zhang, Yu Qin, Yu, Xinliang Zhang, Optimized quantum–well semiconductor optical amplifier for RZ-DPSK signal regeneration, IEEE J. Quantum Electron. 47 (2011) 819–826.
[3] Y. Liu, E. Tangdiongga, Z. Li, H. de Waardt, A.M.J. Koonen, G.D. Khoe, X.W. Shu, I. Bennion, H.J.S. Dorren, Error-free 320-Gb/s all-optical wavelength conversion using a single semiconductor optical amplifier, IEEE J. Lightwave Technol. 25 (2007) 103–108.
[4] J. Xu, X.L. Zhang, J. Mørk, Investigation of patterning effects in ultrafast SOA-based optical switches, IEEE J. Quantum Electron. 46 (2010) 87–94.
[5] J. Dong, X. Zhang, J. Xu, D. Huang, 40 Gb/s all-optical logic NOR and OR gates using a semiconductor optical amplifier: experimental demonstration and theoretical analysis, Opt. Commun. 281 (2008) 1710–1715.
[6] R.P. Webb, J.M. Dailey, R.J. Manning, Pattern compensation in SOA-based gates, Opt. Express 18 (2010) 13502–13509.
[7] Xi Cui Qin, Huang, Xinliang Zhang, Gain recovery acceleration by enhancing differential gain in quantum well semiconductor optical amplifiers, IEEE. Quantum Electron. 47 (2011) 1443–1450.
[8] R. Giller, R.J. Manning, G. Talli, R.P. Webb, M.J. Adams, Analysis of the dimensional dependence of semiconductor optical amplifier recovery speeds, Opt. Exp. 15 (2007) 1773–1782.
[9] P.J.A. Thijs, L.F. Tiemijer, J.J.M. Binsma, T. van Dongen, Progress in long-wavelength strained-layer InGaAs(P) quantum-well semiconductor lasers and amplifiers, IEEE J. Quantum Electron. 30 (1994) 477499.
[10] P.J.A. Thijs, L.F. Tiemijer, P.I. Kuindersma, J.J.M. Binsma, T. van Dongen, High-performance of 1.5 pm wavelength InGaAs–InGaAsP strained quantum-well lasers and amplifiers, IEEE J. Quantum Electron. 27 (1991) 1426–1438.
[11] C. Chang, S.L. Chuang, Modeling of strained quantum-well lasers with spin–orbit coupling, IEEE J. Sel. Top. Quantum Electron. 1 (1995) 218–229.
[12] D. Ahn, S.L. Chuang, The theory of strained-layer quantum well lasers with bandgap renormalization, IEEE J. Quantum Electron. 30 (1994) 350–365.
[13] S.W. Corzine, R.H. Yan, L.A. Coldren, Theoretical gain in strained InGaAdAlGaAs quantum wells including valence-band mixing effects, Appl. Phys. Lett. 57 (1990) 2835–2837.
[14] D. Ahn, T. Yoo, Envelope function calculations of linear and nonlinear optical gains in a strained-layer quantum-well laser, IEEE J. Quantum Electron. 29 (1993) 2864–2872.
[15] J. Mørk, J. Mark, C.P. Seltzer, Carrier heating in InGaAsP laser amplifiers due to two-photon absorption, Appl. Phys. Lett. 64 (1994) 2206–2208.
[16] J. Mørk, A. Mecozzi, Theory of the ultrafast optical response of active semiconductor waveguides, Opt. Soc. Am. B 13 (1996) 1803–1816.
[17] G.P. Agrawal, N.A. Olsson, Amplification and compression of weak picosecond optical pulses by using semiconductor laser amplifiers, Opt. Lett. 14 (1989) 500–502.
[18] Mingjun Xia, H. Ghafouri-Shiraz, Pump current optimization for distortionless amplification in quantum well amplifiers, IEEE J. Lightwave Technol. 33 (2015) 3907–3913.
[19] J.M. Tang, K.A. Shore, Strong picosecond optical pulse propagation in semiconductor optical amplifiers at transparency, IEEE J. Quantum Electron. 34 (1998) 1263–1269.
[20] D. Ahn, Theory of non-Markovian optical gain in quantum-well lasers, Prog. Quant. Electron. 21 (1997) 249–287.
[21] D. Ahn, S.H. Park, E.H. Park, T.K. Yoo, Non-Markovian gain and luminescence of an InGaN–AlInGaN quantum-well with many-body effects, IEEE J. Quantum Electron. 41 (2005) 1253–1259.
[22] Mingjun Xia, H. Ghafouri-Shiraz, A new optical gain model for quantum wells based on quantum well transmission line modelling method, IEEE J. Quantum Electron. 51 (2015).
[23] A. Yariv, Quantum Electronics, 3rd ed., Wiley, New York, 1989.
[24] A.J. Lowery, Transmission-line modelling of semiconductor lasers: the transmission-line laser model, Int. J. Numer. Model. 2 (1989) 249–265.
[25] H. Ghafouri-Shiraz, The Theory of Semiconductor Laser Diodes and Amplifiers: Analysis and Transmission Line Laser Modelling, Imperial College Press, Singapore, 2004.
[26] C.Y.-P. Chao, S.L. Chuang, Spin–orbit-coupling effects on the valence-band structure of strained semiconductor quantum wells, Phys. Rev. E 46 (1992) 411M122.
[27] M. Sugawara, N. Okazalu, T. Fujii, S. Yamazalu, Conduction-band and valence-band structures in strained InGaAs/InP quantum wells on (001) InP substrates, Phys. Rev. E 48 (1993) 8102–8118.
[28] S.L. Chuang, Physics of Optoelectronic Devices, Wiley, New York, 1995.
[29] A.J. Lowery, New dynamic semiconductor laser model based on the transmission line modelling method, IEE Proc. J. 134 (1987) 281–290.